

POD reduced-order unstructured mesh modeling applied to 2D and 3D fluid flow

J. Du^{a,b}, F. Fang^b, C.C. Pain^b, I.M. Navon^{c,*}, J. Zhu^a, D.A. Ham^{b,d}

^a Institute of Atmospheric Physics, Chinese Academy of Sciences, Beijing 100029, China

^b Applied Modeling and Computation Group, Department of Earth Science and Engineering, Imperial College, Prince Consort Road, London SW7 2BP, UK

^c Department of Scientific Computing, Florida State University, Tallahassee, FL 32306-4120, USA

^d Grantham Institute for Climate Change, Imperial College, Prince Consort Road, London SW7 2BP, UK

ARTICLE INFO

Keywords:

POD reduced order model
3D flows
Finite element
Unstructured mesh
Numerical simulation

ABSTRACT

A new scheme for implementing a reduced order model for complex mesh-based numerical models (e.g. finite element unstructured mesh models), is presented. The matrix and source term vector of the full model are projected onto the reduced bases. The proper orthogonal decomposition (POD) is used to form the reduced bases. The reduced order modeling code is simple to implement even with complex governing equations, discretization methods and nonlinear parameterizations. Importantly, the model order reduction code is independent of the implementation details of the full model code. For nonlinear problems, a perturbation approach is used to help accelerate the matrix equation assembly process based on the assumption that the discretized system of equations has a polynomial representation and can thus be created by a summation of pre-formed matrices.

In this paper, by applying the new approach, the POD reduced order model is implemented on an unstructured mesh finite element fluid flow model, and is applied to 3D flows. The error between the full order finite element solution and the reduced order model POD solution is estimated. The feasibility and accuracy of the reduced order model applied to 3D fluid flows are demonstrated.

© 2012 Elsevier Ltd. All rights reserved.

1. Introduction

The major issue in large scale complex modeling is that of reducing the computational cost while preserving numerical accuracy. Using reduced-order modeling amounts to projecting the high-fidelity model onto a reduced space basis. This yields a set of ordinary differential equations in time, requiring a greatly reduced computational effort [1,2]. Among the existing approaches, the proper orthogonal decomposition (POD) method provides an efficient means of deriving the reduced basis for high-dimensional nonlinear flow systems. This technique provides a low-dimensional description of the time-dependent dynamic system in an optimal way resulting in capture of the greatest possible energy of the system. The POD method has been widely and successfully applied to signal analysis and pattern recognition [3] as Karhounen–Loeve expansions, statistics [4] as principal component analysis (PCA), and geophysical fluid dynamics and meteorology [5,6] as empirical orthogonal functions (EOF). Some reduced order finite difference models and mixed finite element formulations based on the POD method [7–12] were also developed.

* Corresponding author. Tel.: +1 850 644 6560; fax: +1 850 644 0098.
E-mail address: inavon@fsu.edu (I.M. Navon).

Most existing approaches for the implementation of POD reduced order models require an intimate knowledge of complex governing equations and spatial discretization methods used in discretizing the full model. The POD reduced order models are derived by projecting the original partial differential equations (PDEs) onto the reduced space, then discretizing. For complex mesh based nonlinear models, the reduced order code (including the reduced-basis discretization procedure) is not simple to implement while retaining the advanced numerical techniques used in the full model (e.g. unstructured mesh, numerical stabilization schemes, balance conservation etc.). The computational efficiency in forming and solving the POD reduced-order systems is limited to the linear or bilinear problems [13,14].

More recently, the discrete empirical interpolation method (DEIM) in conjunction with POD improves the efficiency of the POD approximation and achieves a complexity reduction of the nonlinear term in the full model with a complexity proportional to the number of reduced variables [15–18]. In this work, a new approach is proposed to derive the POD reduced order model by projecting the matrix and source term vector of the full discrete model onto the reduced space. The implementation of reduced order modeling codes involves only the matrix vector multiplication of the full model. Importantly, the code is largely independent of the implementation details of the original equations. For nonlinear problems, a perturbation approach is used to help accelerate the matrix equation assembly process, based on the assumption that the discretized system of equations has a polynomial representation and can thus be created by a summation of pre-formed matrices.

By using the new approach, a POD based reduced order model has been developed for an unstructured fluid model, i.e. the Imperial College Ocean Model (*Fluidity-ICOM*) which can simultaneously resolve both small and large scale ocean flows while smoothly varying the resolution and conforming to complex coastlines and bathymetry [19,20]. This discrete POD model retains the advanced numerical techniques as the forward model continues to be developed.

Adaptive unstructured mesh models offer significant advantages over traditional models and are expected to revolutionize the way multi-scale modeling is performed because they are the only techniques that can simultaneously resolve both small and large scale flows, thus ensuring that areas of fine resolution are used only when and where they are required. The key objective of using such meshes is to reduce the overall computational cost and increase the accuracy of solutions, hence increasing the accuracy of snapshots which are used to form the POD bases for the POD reduced order models.

This article is organized as follows. Section 2 describes the underlying equations of the fluid model. In Section 3, a POD reduced order model is derived. Section 4 provides the error analysis between the POD reduced model and the full finite element model. Section 5 presents some numerical results and demonstrates the feasibility of the POD method as well as the CPU time gained by applying the POD model reduction in the present form.

2. Description of the fluid model

The three-dimensional (3D) non-hydrostatic Boussinesq equations used in the underlying fluid model are presented as follows

$$\nabla \cdot \mathbf{u} = 0, \tag{2.1}$$

$$\rho_0 \frac{\partial \mathbf{u}}{\partial t} = -\nabla p - \mathbf{u} \cdot \nabla \mathbf{u} - f \mathbf{k} \times \mathbf{u} - \rho g \mathbf{k} + \nabla \cdot \boldsymbol{\tau}, \tag{2.2}$$

$$\frac{\partial T}{\partial t} + \nabla \cdot (\mathbf{u}T) = \nabla \cdot (\kappa \nabla T), \tag{2.3}$$

$$\rho = \rho_0(1 - \alpha(T - T_0)), \tag{2.4}$$

where $\mathbf{u} = (u, v, w)^T = (u_1, u_2, u_3)^T$ is the velocity vector, p is the perturbation pressure ($p := p/\rho_0$, ρ_0 is the constant reference density), f is the Coriolis force, g is the acceleration due to gravity, T is the temperature. ρ is the density which satisfies the linear equation of state. ρ_0 and T_0 are the reference state values. α is the thermal expansion coefficient. The stress tensor $\boldsymbol{\tau}$ is used to represent the viscous terms and is related to the deformation rate tensor S_{ij} as

$$\tau_{ij} = 2\mu_{ij}S_{ij}, \quad 1 \leq i, j \leq 3, \tag{2.5}$$

$$S_{ij} = \frac{1}{2} \left(\frac{\partial u_i}{\partial x_j} + \frac{\partial u_j}{\partial x_i} \right) - \frac{1}{3} \sum_{k=1}^3 \frac{\partial u_k}{\partial x_k}, \quad 1 \leq i, j \leq 3, \tag{2.6}$$

with no summation over repeated indices where $\mathbf{x} = (x, y, z)^T$ is the Cartesian coordinate system and the viscosities μ_{ij} are constants. The horizontal viscosities μ_{11} and μ_{22} are allowed to assume two different, uniform values, and the off-diagonal components of $\boldsymbol{\tau}$ satisfy $\mu_{ij} = (\mu_{ii}\mu_{jj})^{1/2}$. In principle, coupling of the momentum and continuity equations results in an extremely large system of equations, for which an efficient solution strategy is difficult to achieve. Therefore, a technique (e.g. a projection method) is used in which the pressure and velocity variables are solved independently, thus reducing the total dimension of the equation system [20].

By applying the finite element method [20], the momentum equations and the continuity equation are rewritten as follows:

$$\int_{\Omega} M_i \nabla \cdot u d\Omega = 0, \quad (2.7)$$

$$\int_{\Omega} N_i \rho_0 \frac{\partial u}{\partial t} d\Omega = \int_{\Omega} N_i (-\nabla p - \mathbf{u} \cdot \nabla \mathbf{u} - f \mathbf{k} \times \mathbf{u} - \rho g \mathbf{k} + \nabla \cdot \boldsymbol{\tau}) d\Omega, \quad (2.8)$$

where Ω denotes the computational domain, N_i and M_i are the test functions for momentum and pressure, respectively.

The momentum equation discretized in space can be rewritten in a matrix form:

$$M_u \frac{\partial u}{\partial t} + A(u)u + Ku + Cp = 0, \quad (2.9)$$

where M_u is the velocity mass matrix. $A(u)$ is the advection matrix related to the nonlinear term in the momentum equation. K is the matrix related to the rest of the linear terms of velocity. C is the pressure gradient matrix.

Using the θ -method to discretize the above equations in time yields:

$$M_u \frac{u^{n+1} - u^n}{\Delta t} + A(u^n)u^{n+\theta_m} + Ku^{n+\theta_m} + Cp^{n+\theta_p} = 0, \quad (2.10)$$

where

$$u^{n+\theta_m} = \theta_m u^{n+1} + (1 - \theta_m)u^n, \quad (2.11)$$

and

$$p^{n+\theta_p} = \theta_p p^{n+1} + (1 - \theta_p)p^n, \quad (2.12)$$

where $0 \leq \theta_m \leq 1$ and $0 \leq \theta_p \leq 1$.

Eq. (2.10) is first solved with an initial guess pressure $p_*^{n+\theta_p}$ replacing $p^{n+\theta_p}$, defining:

$$p_*^{n+\theta_p} = \theta_p p_*^{n+1} + (1 - \theta_p)p^n, \quad (2.13)$$

where p_*^{n+1} could be obtained from the previous time step or an initial pressure-Poisson solve. Denote u_*^{n+1} as the most recent solve for velocity. So, instead of Eq. (2.10) one could consider solving

$$M_u \frac{u_*^{n+1} - u^n}{\Delta t} + A(u^n)u_*^{n+\theta_m} + Ku_*^{n+\theta_m} + Cp_*^{n+\theta_p} = 0, \quad (2.14)$$

where now

$$u_*^{n+\theta_m} = \theta_m u_*^{n+1} + (1 - \theta_m)u^n. \quad (2.15)$$

Then consider a pressure-correction Δp defined as:

$$\Delta \hat{p} = p^{n+1} - p_*^{n+1} \quad (2.16)$$

where \hat{p}^{n+1} satisfies

$$M_u \frac{\hat{u}^{n+1} - u^n}{\Delta t} + A(u^n)u_*^{n+\theta_m} + Ku_*^{n+\theta_m} + C\hat{p}_*^{n+\theta_p} = 0, \quad (2.17)$$

where

$$\Delta \hat{p}^{n+\theta_p} = \theta_p \hat{p}^{n+1} + (1 - \theta_p)p^n. \quad (2.18)$$

Subtracting (2.14) from (2.17), yields

$$M_u \frac{\hat{u}^{n+1} - u_*^{n+1}}{\Delta t} + \theta_p C \Delta p = 0. \quad (2.19)$$

Multiplying (2.19) by $C^T M_u^{-1}$, yields

$$-C^T \frac{\hat{u}^{n+1} - u_*^{n+1}}{\Delta t} = \theta_p C^T M_u^{-1} C \Delta p = 0. \quad (2.20)$$

To accurately represent the local flow around steep topography, no hydrostatic assumption is made here. The pressure variable is split into a non-geostrophic and a geostrophic component. This allows the accurate representation of the hydrostatic/geostrophic balance [20,19].

3. POD-reduced model

3.1. Proper orthogonal decomposition

Let V represent the model variables (e.g. u, v, p). The ensemble of snapshots sampled at designated time steps $\{V^l\}_{l=1}^{\mathcal{L}} = \{V_i^l\}_{i=1}^{\mathcal{N}} (1 \leq i \leq \mathcal{N}) (\mathcal{L} \leq \mathcal{N}^T)$ can be expressed as follows $\mathcal{N} \times \mathcal{L}$ matrix \mathbf{A}_V , where \mathcal{N} is the number of nodes, \mathcal{N}^T is the number of time steps, and \mathcal{L} is the number of snapshots, respectively.

$$\mathbf{A}_V = \begin{pmatrix} V_1^1 & V_1^2 & \dots & V_1^{\mathcal{L}} \\ V_2^1 & V_2^2 & \dots & V_2^{\mathcal{L}} \\ \vdots & \vdots & \vdots & \vdots \\ V_{\mathcal{N}}^1 & V_{\mathcal{N}}^2 & \dots & V_{\mathcal{N}}^{\mathcal{L}} \end{pmatrix}. \tag{3.1}$$

The average of the ensemble of snapshots $\{\bar{V}_i\}_{i=1}^{\mathcal{N}}$ is defined as

$$\bar{V}_i = \frac{1}{\mathcal{L}} \sum_{l=1}^{\mathcal{L}} V_i^l, \quad 1 \leq i \leq \mathcal{N}. \tag{3.2}$$

Taking the deviation from the mean of the variables yields

$$\widehat{V}_i^l = V_i^l - \bar{V}_i, \quad 1 \leq i \leq \mathcal{N}, \quad 1 \leq l \leq \mathcal{L}, \tag{3.3}$$

which constructs a $\mathcal{N} \times \mathcal{L}$ matrix $\mathbf{A} = \{\widehat{V}_i^l\}_{i=1}^{\mathcal{N}}$.

The essence of the POD method consists in finding a set of orthogonal basis functions $\{\phi_i\} (i = 1, \dots, \mathcal{L})$ to maximize the following representation

$$\frac{1}{\mathcal{L}} \sum_{i=1}^{\mathcal{L}} |\langle \widehat{V}^i, \phi_i \rangle_{L^2}|^2, \tag{3.4}$$

subject to

$$\langle \phi_i, \phi_j \rangle_{L^2} = 1, \quad i = j, \tag{3.5}$$

$$\langle \phi_i, \phi_j \rangle_{L^2} = 0, \quad i \neq j, \tag{3.6}$$

where $i, j = 1, 2, \dots, \mathcal{L}$ and the inner product is defined in the L^2 space as $\langle f, g \rangle_{L^2} = \int_{\Omega} fg d\Omega$ in which f and g are two real functions defined on the space Ω [21].

Using the L^2 inner product, the above optimization problem becomes

$$\max_{\phi_i \in L^2} \frac{1}{\mathcal{L}} \sum_{i=1}^{\mathcal{L}} |\langle \widehat{V}^i, \phi_i \rangle_{L^2}|^2 = \max_{\phi_i \in L^2} \frac{1}{\mathcal{L}} \sum_{i=1}^{\mathcal{L}} \int_{\Omega} \widehat{V}^i \phi_i d\Omega. \tag{3.7}$$

Since the basis functions can be represented as a linear combination of the solution snapshots:

$$\phi = \sum_{i=1}^{\mathcal{L}} a_i \widehat{V}^i, \tag{3.8}$$

the optimization problem can be represented by the following eigenvalue problem

$$\mathbf{D}\mathbf{x} = \lambda\mathbf{x}, \tag{3.9}$$

where

$$\mathbf{D} = \{c_{i,j}\}_{i,j=1}^{\mathcal{N}} = \left\{ \int_{\Omega} (\widehat{V}^i)^T \widehat{V}^j d\Omega \right\}_{i,j=1}^{\mathcal{N}} = \mathbf{A}\mathbf{A}^T. \tag{3.10}$$

In order to solve the above eigenvalue problem, we employ the Singular Value Decomposition (SVD) to obtain an optimal representation for \mathbf{A} [22]. SVD is an important tool in the construction of optimal bases for reduced order approximation. For the matrix $\mathbf{A} \in R^{\mathcal{N} \times \mathcal{L}}$, there exists the SVD

$$\mathbf{A} = \mathbf{U} \begin{pmatrix} \mathbf{S} & 0 \\ 0 & 0 \end{pmatrix} \mathbf{W}^T, \tag{3.11}$$

where $\mathbf{U} \in R^{\mathcal{N} \times \mathcal{N}}$ and $\mathbf{W} \in R^{\mathcal{L} \times \mathcal{L}}$ are all orthogonal matrices, $\mathbf{S} = \text{diag}\{\sigma_1, \sigma_2, \dots, \sigma_{\ell}\} \in R^{\ell \times \ell}$ is a diagonal matrix corresponding to \mathbf{A} , and $\sigma_i (i = 1, 2, \dots, \ell)$ are positive singular values where ℓ denotes the number of positive singular

values. The matrices $\mathbf{U} = (\phi_1, \phi_2, \dots, \phi_N) \in R^{N \times N}$ and $\mathbf{W} = (\varphi_1, \varphi_2, \dots, \varphi_L) \in R^{L \times L}$ contain the orthogonal eigenvectors to the \mathbf{AA}^T and $\mathbf{A}^T\mathbf{A}$, respectively. The columns of these eigenvector matrices are organized corresponding to the singular values σ_i and are arranged in \mathbf{S} descending order. Since the number of mesh points is much larger than that of the transient points, i.e., $N \gg L$, the order N of the matrix \mathbf{AA}^T is also much larger than the order L of the matrix $\mathbf{A}^T\mathbf{A}$, however, their null eigenvalues are identical.

Therefore, we may solve the eigenvalue equation corresponding to the matrix $\mathbf{A}^T\mathbf{A}$ to find the eigenvectors φ_j ($j = 1, 2, \dots, \ell$),

$$\mathbf{A}^T\mathbf{A}\varphi_j = \lambda_i\varphi_j, \quad j = 1, 2, \dots, \ell. \tag{3.12}$$

Since the singular values of the SVD method are associated to the eigenvalues of the matrices \mathbf{AA}^T and $\mathbf{A}^T\mathbf{A}$ in such a manner that $\lambda_i = \sigma_i^2$ ($i = 1, 2, \dots, \ell$), we may obtain ℓ ($\ell \leq L$) eigenvectors $\{\varphi_j\}_{j=1}^\ell$ corresponding to the non-null eigenvalues for the matrix \mathbf{AA}^T by

$$\phi_j = \frac{1}{\sigma_j}\mathbf{A}\varphi_j, \quad j = 1, 2, \dots, \ell, \tag{3.13}$$

which can generate a space \mathcal{V} defined by $\mathcal{V} = \text{span}\{\phi_1, \dots, \phi_\ell\}$.

Our objective is to choose an optimal subspace of \mathcal{V} which is of as low a dimension, m , as possible, while still maintaining a good approximation of the original data set. We write $\mathcal{V}_m = \text{span}\{\phi_1, \dots, \phi_m\}$ for this subspace and refer to the vectors ϕ_i as *POD modes*. The quality of the approximation is measured using the relative information content [23,24], usually referred to as *energy*, defined as:

$$I(m) = \frac{\sum_{i=1}^m \lambda_i}{\sum_{i=1}^\ell \lambda_i}. \tag{3.14}$$

The goal is to choose the smallest m such that $I(m)$ is still sufficiently close to 1. For example, if the subspace \mathcal{V}_m should contain a percentage γ of the information in \mathcal{V} , then one should choose m such that [25]

$$m = \text{argmin} \left\{ I(m) : I(m) \geq \frac{\gamma}{100} \right\}. \tag{3.15}$$

In many applications, including fluid dynamics, one observes an exponential decrease of the singular eigenvalues [26], there is a good chance to obtain low-order approximate models.

Hence, the state variable can be represented by the linear combination of the retained POD basis functions as follows:

$$V(\mathbf{x}, t) = \bar{V} + \sum_{i=1}^m \alpha_i(t)\phi_i(\mathbf{x}), \tag{3.16}$$

where $\alpha_i(t)$ ($i = 1, \dots, m$) are the POD coefficients corresponding to every POD basis function.

3.2. Implementation of the POD reduced order model for the 3D unstructured mesh fluid model

In this study, a POD reduced order model is developed for the 3D unstructured mesh fluid model (*Fluidity-ICOM*, developed by AMCG, Imperial College London) that can simultaneously resolve both small- and large-scale fluid flows while smoothly varying model resolution and conforming to complex coastlines and bathymetry [19,20,27]. The model employs 3D anisotropic mesh adaptivity to resolve and reveal fine scale features as they develop while reducing resolution elsewhere. Being non-hydrostatic it can cope with steep topography. The model consists of the 3D continuity and non-hydrostatic Boussinesq equations.

The variables to be solved can be expressed as an expansion of the first few POD basis functions $\phi^u = \{\phi_1^u, \dots, \phi_{N_{\text{pod}}}^u\}$, $\phi^v = \{\phi_1^v, \dots, \phi_{N_{\text{pod}}}^v\}$, $\phi^w = \{\phi_1^w, \dots, \phi_{N_{\text{pod}}}^w\}$ and $\phi^p = \{\phi_1^p, \dots, \phi_{M_{\text{pod}}}^p\}$:

$$u(\mathbf{x}, t) = \overline{u(\mathbf{x})} + \sum_{i=1}^{N_{\text{pod}}} \alpha_i^u(\mathbf{t})\phi_i^u(\mathbf{x}), \tag{3.17}$$

$$v(\mathbf{x}, t) = \overline{v(\mathbf{x})} + \sum_{i=1}^{N_{\text{pod}}} \alpha_i^v(\mathbf{t})\phi_i^v(\mathbf{x}), \tag{3.18}$$

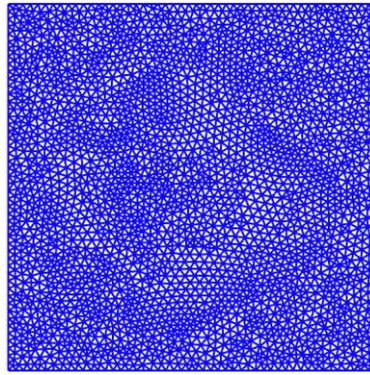


Fig. 1. Unstructured mesh.

$$w(\mathbf{x}, t) = \overline{w(\mathbf{x})} + \sum_{i=1}^{\mathcal{N}^{\text{pod}}} \alpha_i^w(\mathbf{t}) \phi_i^w(\mathbf{x}), \tag{3.19}$$

$$p(\mathbf{x}, t) = \overline{p(\mathbf{x})} + \sum_{i=1}^{\mathcal{M}^{\text{pod}}} \alpha_i^p(\mathbf{t}) \phi_i^p(\mathbf{x}), \tag{3.20}$$

where u, v, w, p are the model variables, in finite element $\bar{u} = \sum_{j=1}^{\mathcal{N}} N_j(\mathbf{x}) \bar{u}_j$, $\bar{v} = \sum_{j=1}^{\mathcal{N}} N_j(\mathbf{x}) \bar{v}_j$, $\bar{w} = \sum_{j=1}^{\mathcal{N}} N_j(\mathbf{x}) \bar{w}_j$ and $\bar{p} = \sum_{j=1}^{\mathcal{N}} N_j(\mathbf{x}) \bar{p}_j$ are the mean of the ensemble of snapshots for the variables of the equations, $\alpha_i^u, \alpha_i^v, \alpha_i^w$ ($1 \leq i \leq \mathcal{N}^{\text{pod}}$) and α_i^p ($1 \leq i \leq \mathcal{M}^{\text{pod}}$) are the coefficients to be determined, and $\alpha_i^u(0), \alpha_i^v(0), \alpha_i^w(0), \alpha_i^p(0)$ are the coefficients of the initial condition, \mathcal{N}^{pod} and \mathcal{M}^{pod} are the number of POD bases used for velocity and pressure respectively. The POD basis functions are expressed as a finite element expansion:

$$\phi_m^u = \sum_{j=1}^{\mathcal{N}} N_{x_t j} \phi_{mj}^u, \quad \phi_m^v = \sum_{j=1}^{\mathcal{N}} N_{x_t j} \phi_{mj}^v, \quad \phi_m^w = \sum_{j=1}^{\mathcal{N}} N_{x_t j} \phi_{mj}^w, \quad 1 \leq m \leq \mathcal{N}^{\text{pod}}, \tag{3.21}$$

$$\phi_m^p = \sum_{j=1}^{\mathcal{N}} N_{x_t j} \phi_{mj}^p, \quad 1 \leq m \leq \mathcal{M}^{\text{pod}}. \tag{3.22}$$

The system equation of the finite element scheme for the fluid model is represented as follows:

$$\begin{pmatrix} \mathbf{B} & \mathbf{C} \\ \mathbf{C}^T & \mathbf{0} \end{pmatrix} \begin{pmatrix} \mathbf{u} \\ p \end{pmatrix} = \begin{pmatrix} \mathbf{b} \\ \mathbf{0} \end{pmatrix}, \tag{3.23}$$

in which $\mathbf{B} \in \mathcal{R}^{3\mathcal{N} \times 3\mathcal{N}}$ represents the system matrix of the velocity $\mathbf{u} = (u, v, w)^T$, $\mathbf{C} \in \mathcal{R}^{3\mathcal{N} \times 3\mathcal{M}}$ is the system matrix of pressure p , and \mathbf{b} is the source vector.

In a manner analogous to the Galerkin method, by taking the POD basis function as the test function and projecting the original discrete model (3.23) onto the reduced space (i.e. multiplying the rows and columns of the matrix in (3.23) by the POD basis functions ϕ_m^u and ϕ_m^p), the POD discrete model of (3.23) is obtained:

$$\begin{pmatrix} \mathbf{B}^{\text{pod}} & \mathbf{C}^{\text{pod}} \\ (\mathbf{C}^{\text{pod}})^T & \mathbf{0} \end{pmatrix} \begin{pmatrix} \alpha^u \\ \alpha^p \end{pmatrix} = \begin{pmatrix} \mathbf{b}^{\text{pod}} \\ \mathbf{0} \end{pmatrix}, \tag{3.24}$$

where

$$\mathbf{B}^{\text{pod}} = \phi^{uT} \mathbf{B} \phi^u, \quad \mathbf{C}^{\text{pod}} = \phi^{pT} \mathbf{C} \phi^p, \quad \mathbf{b}^{\text{pod}} = \phi^{uT} \mathbf{b}, \tag{3.25}$$

and $\phi^u = (\phi^u, \phi^v, \phi^w) \in \mathcal{R}^{\mathcal{N} \times 3\mathcal{N}^{\text{pod}}}$, $\phi^p \in \mathcal{R}^{\mathcal{N} \times 3\mathcal{M}^{\text{pod}}}$, $\mathbf{B}^{\text{pod}} \in \mathcal{R}^{3\mathcal{N}^{\text{pod}} \times 3\mathcal{N}^{\text{pod}}}$ and $\mathbf{C}^{\text{pod}} \in \mathcal{R}^{3\mathcal{M}^{\text{pod}} \times 3\mathcal{M}^{\text{pod}}}$.

3.3. Acceleration of the POD reduced model

For a nonlinear simulation, the matrix \mathbf{B} is model variable and time dependent, i.e. $\mathbf{B} = \mathbf{B}(\mathbf{u}(\mathbf{x}), t)$. It is time consuming to calculate \mathbf{B} at each time level. To speed up the matrix equation assembly process, the matrix \mathbf{B} is constructed here by a set of sub-matrices independent of time. Recalling the POD representations of the state variables (see Eqs. (3.17)–(3.20)) on

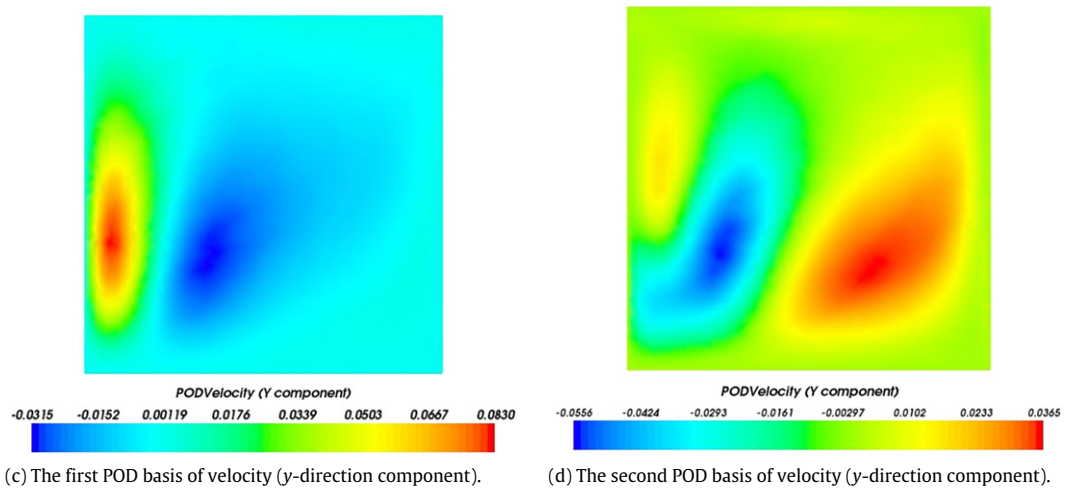
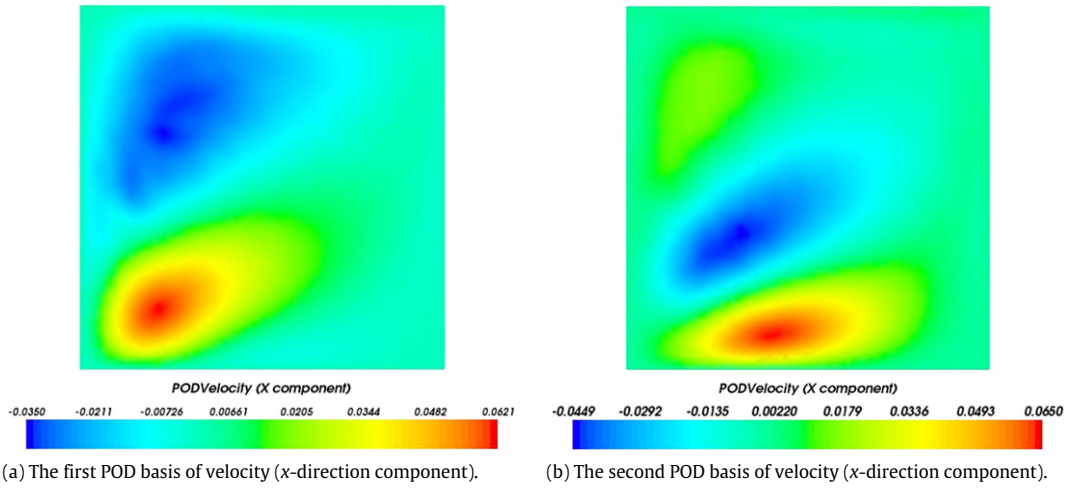


Fig. 2. The first and second POD basis functions of velocity components.

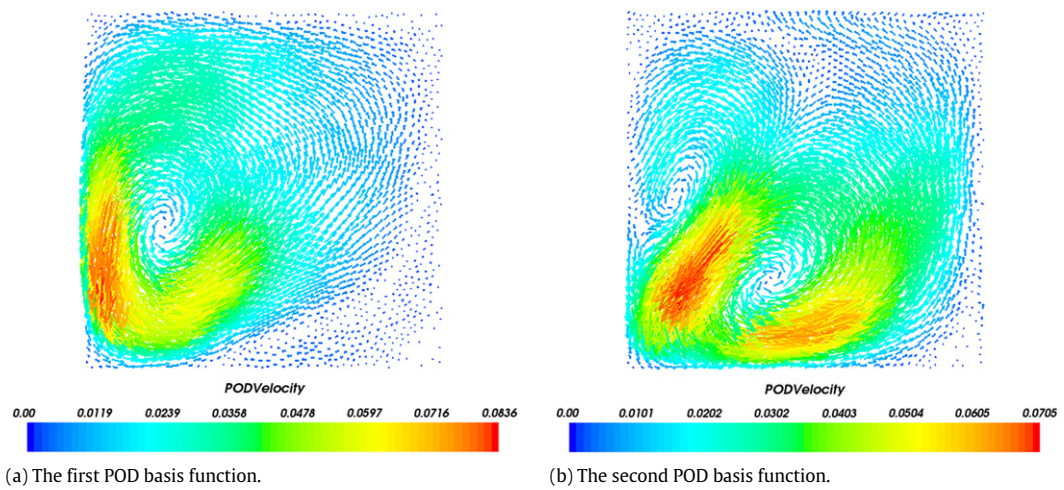


Fig. 3. The first and second POD basis functions of velocity.

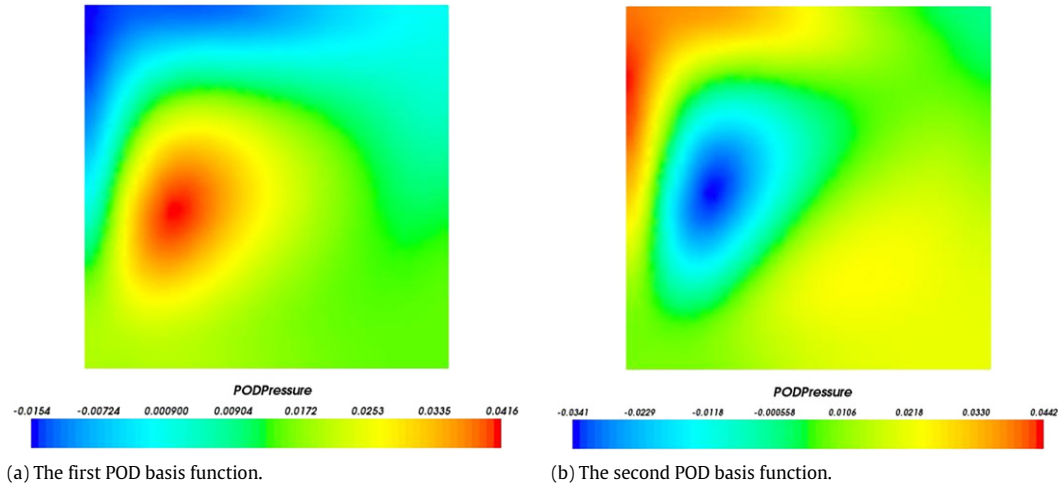


Fig. 4. The first and second POD basis functions of pressure.

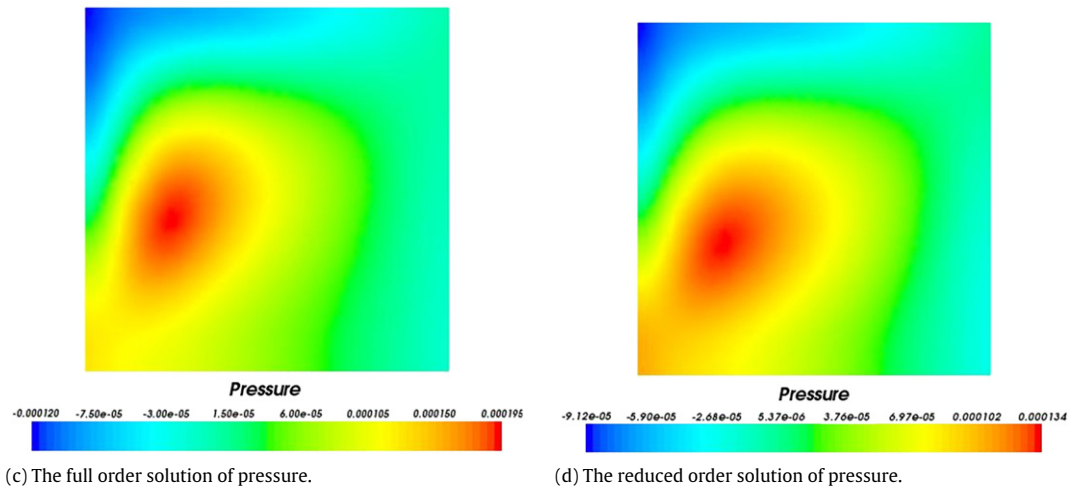
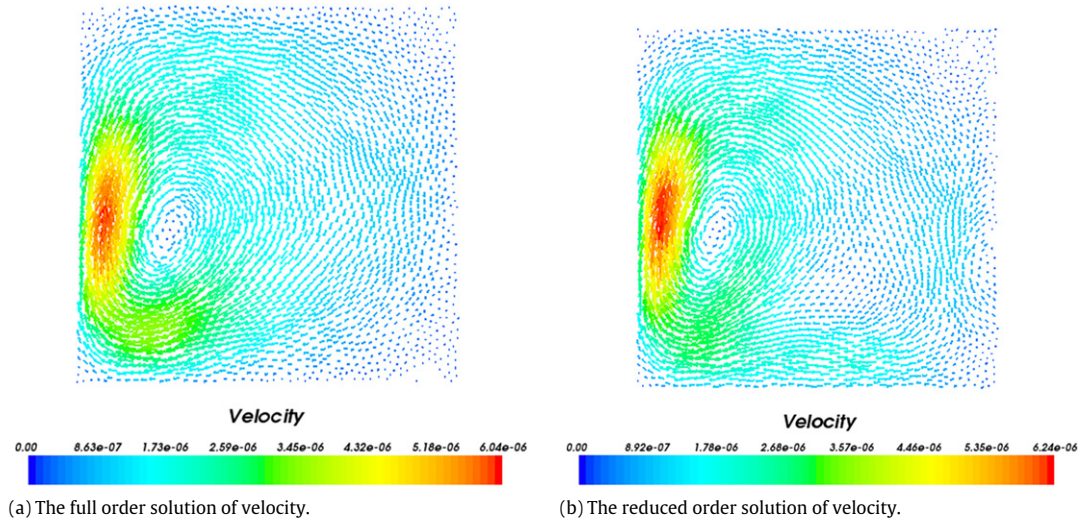


Fig. 5. The full model solution and the reduced order solution of velocity and pressure at $t = 0.16$.

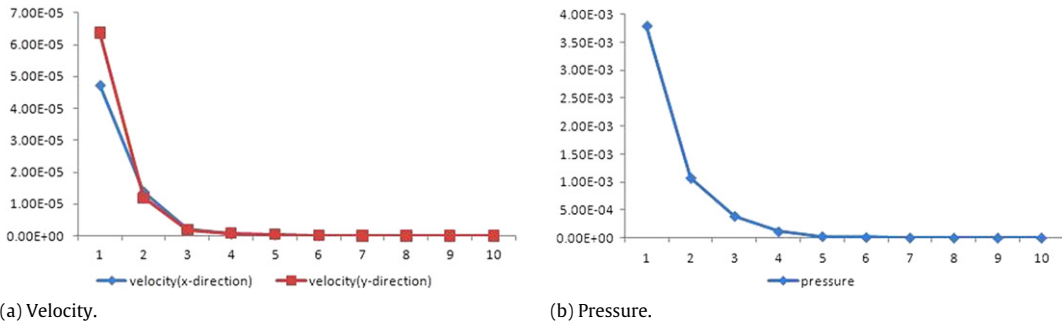


Fig. 6. The eigenvalues in a descending order.

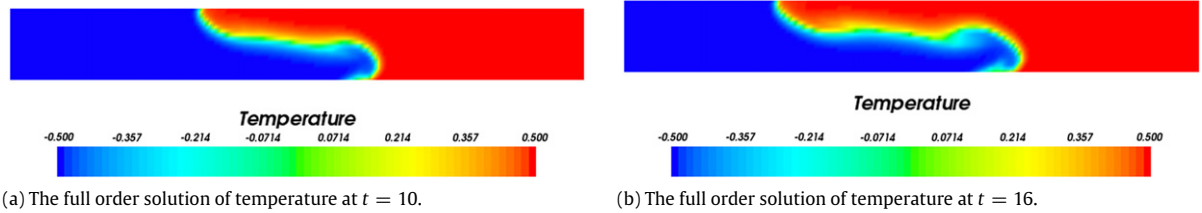


Fig. 7. The full order solutions of temperature at $t = 10$ and $t = 16$.

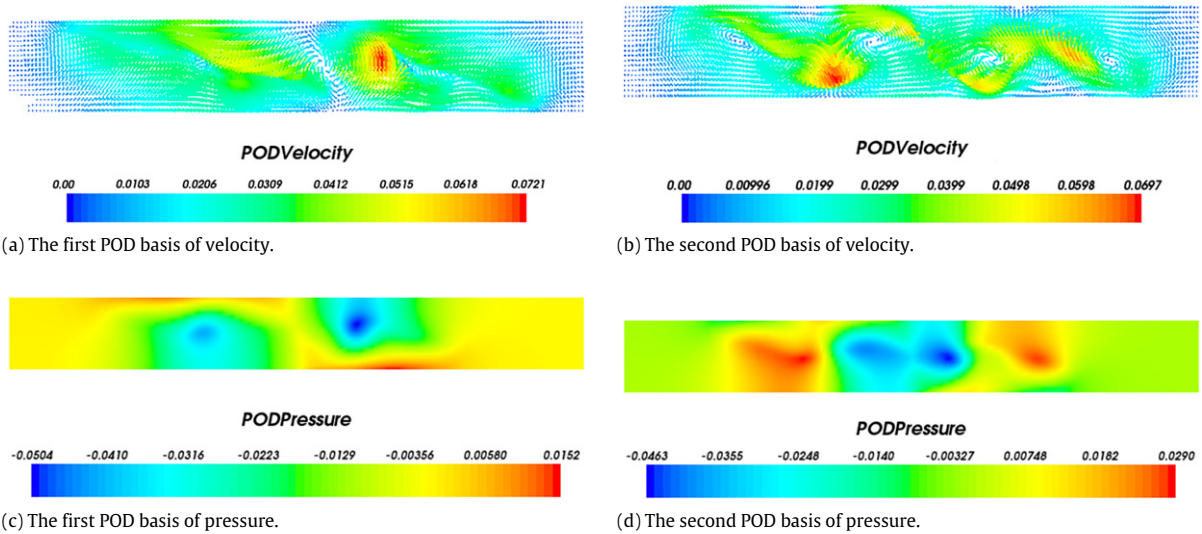


Fig. 8. The first and second POD basis functions of velocity and pressure.

the assumption that the discretized system of equations has a polynomial representation (e.g. for quadratic problems), the matrix $B(\mathbf{u}(\mathbf{x}), t)$ can be expressed as:

$$B(u, v, w, t) = \bar{B} + \sum_{i=1}^{\mathcal{N}^{\text{pod}}} \hat{B}_i, \tag{3.26}$$

and

$$\hat{B}_i = \begin{pmatrix} \alpha_i^u \hat{B}_i^u & 0 & 0 \\ 0 & \alpha_i^v \hat{B}_i^v & 0 \\ 0 & 0 & \alpha_i^w \hat{B}_i^w \end{pmatrix}, \tag{3.27}$$

where $\hat{B}_i^u = B(\phi_i^u)$, $\hat{B}_i^v = B(\phi_i^v)$, $\hat{B}_i^w = B(\phi_i^w)$, $\bar{B} = B(\bar{\mathbf{u}})$ ($\hat{B}_i^u, \hat{B}_i^v, \hat{B}_i^w, \bar{B} \in \mathcal{R}^{\mathcal{N} \times \mathcal{N}}$).

A new perturbation approach is employed to calculate the sub-matrices prior to the POD simulation. By applying a perturbation to the mean velocity $\bar{\mathbf{u}}$, i.e. setting $\alpha^u = \{0, \dots, \epsilon, \dots, 0\}$ (here, $\alpha_i^u = \epsilon$), $\alpha^v = \{0, \dots, 0, \dots, 0\}$ and

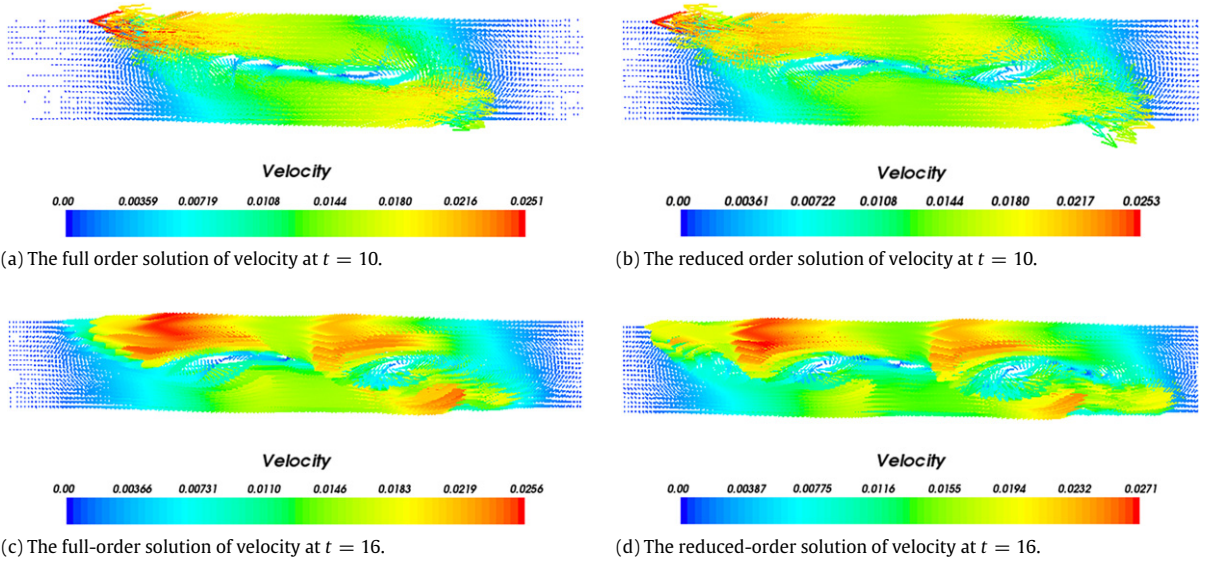


Fig. 9. The full model solution and the reduced order solution of velocity at $t = 10$ and $t = 16$.

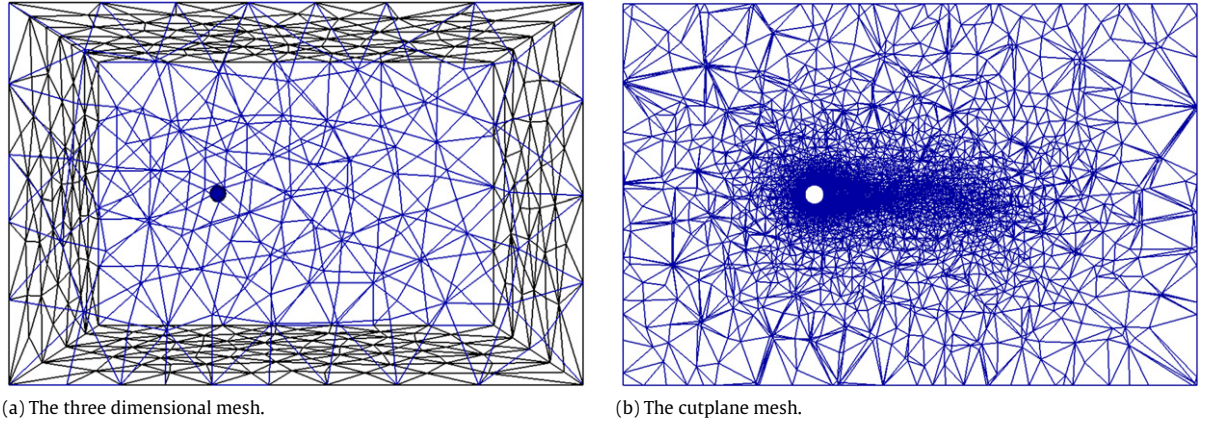


Fig. 10. Unstructured mesh.

$\alpha^w = \{0, \dots, 0, \dots, 0\}$, the perturbed velocity is

$$\begin{aligned} u(\mathbf{x}, t) &= \overline{u(\mathbf{x})} + \epsilon \phi_i^u, \\ v(\mathbf{x}, t) &= \overline{v(\mathbf{x})}, \\ w(\mathbf{x}, t) &= \overline{w(\mathbf{x})}. \end{aligned} \tag{3.28}$$

Taking into account (3.26) yields

$$\mathbf{B}(\overline{u} + \epsilon \phi_i^u, \overline{v}, \overline{w}, t) = \overline{\mathbf{B}}(\overline{u}, \overline{v}, \overline{w}) + \epsilon \widehat{\mathbf{B}}_i^u. \tag{3.29}$$

The sub-matrix $\widehat{\mathbf{B}}_i^u$ is then calculated as:

$$\widehat{\mathbf{B}}_i^u = \frac{1}{\epsilon} (\mathbf{B}(\overline{u} + \epsilon \phi_i^u, \overline{v}, \overline{w}, t) - \overline{\mathbf{B}}(\overline{u}, \overline{v}, \overline{w})). \tag{3.30}$$

In a manner analogous to $\widehat{\mathbf{B}}_i^u$, the sub-matrices $\widehat{\mathbf{B}}_i^v$ and $\widehat{\mathbf{B}}_i^w$ can be pre-computed. Projecting $\widehat{\mathbf{B}}_i$ and $\overline{\mathbf{B}}$ (see Eq. (3.25)) onto the reduced space, yields

$$\widehat{\mathbf{B}}_i^{\text{pod}} = \phi^{uT} \widehat{\mathbf{B}}_i \phi^u, \quad \overline{\mathbf{B}}^{\text{pod}} = \phi^{uT} \overline{\mathbf{B}} \phi^u, \tag{3.31}$$

where $\widehat{\mathbf{B}}_i^{\text{pod}} \in \mathcal{R}^{3, \mathcal{N}^{\text{pod}} \times 3, \mathcal{N}^{\text{pod}}}$ and $\overline{\mathbf{B}}^{\text{pod}} \in \mathcal{R}^{3, \mathcal{N}^{\text{pod}} \times 3, \mathcal{N}^{\text{pod}}}$ are stored prior to the POD simulation.

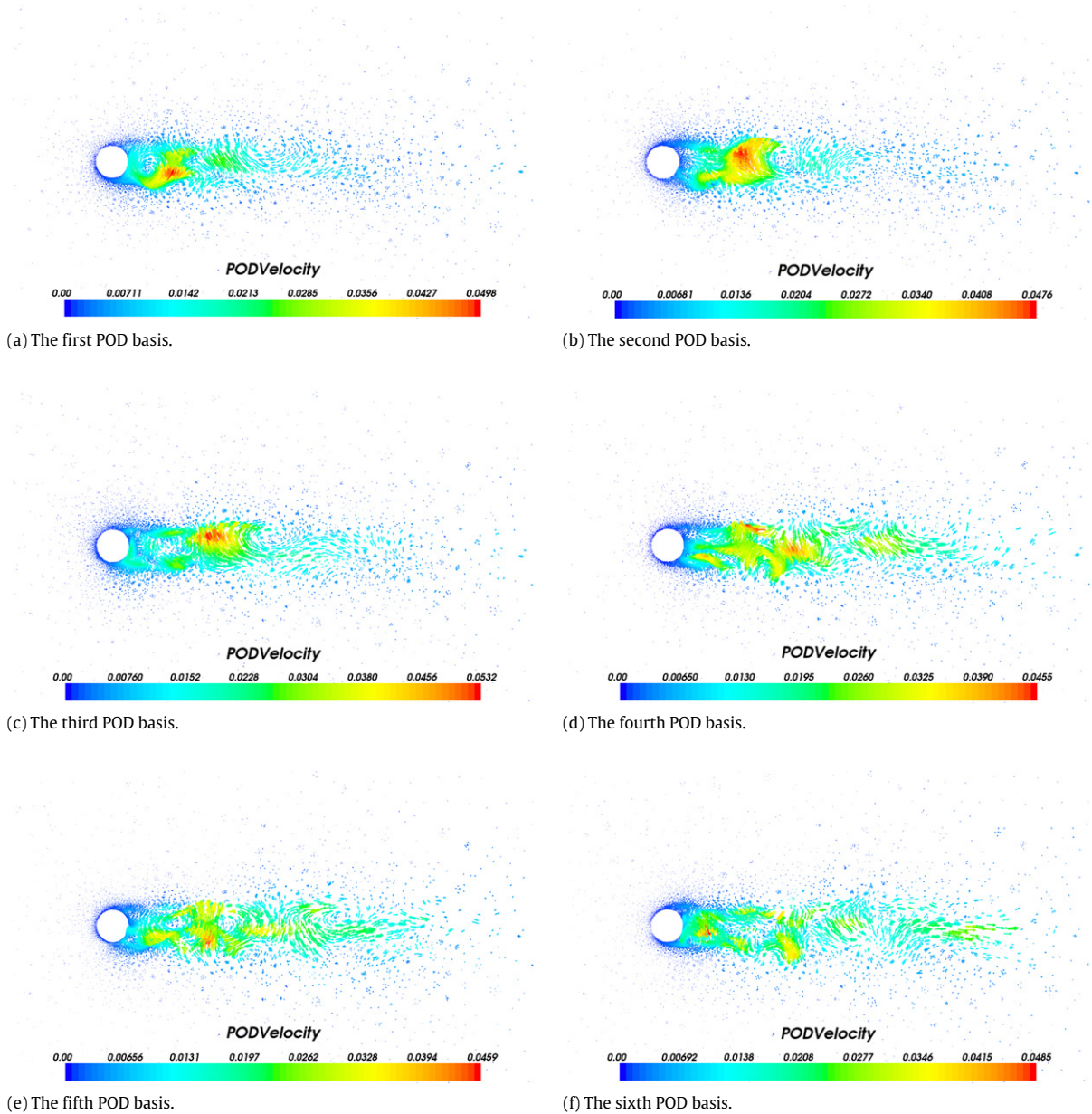


Fig. 11. The first 6 POD basis functions of velocity in the descending order of corresponding eigenvalues.

4. Numerical simulations

In this section, some 2D numerical tests including the gyre case for the fluid model [13] and the lock exchange case are carried out to demonstrate the feasibility and efficiency of the POD method, as well as the efficiency of the speed-up process in the unstructured mesh finite element scheme. Numerical results of POD reduced order modeling applied to the 3D model of flow past sphere with moderate Reynolds number are also presented.

4.1. The 2D gyre case

The POD reduced order model is tested with a barotropic wind-driven gyre problem in a computational domain, $L = 1000$ km by 1000 km with a depth of $H = 500$ m. The problem is non-dimensionalized with the maximum Sverdrup balance velocity

$$\beta H \rho_0 v = \frac{\partial \tau}{\partial y} \leq \frac{\tau_0 \pi}{L} \Rightarrow v \leq 3.5 \times 10^{-2} \text{ m s}^{-1}, \tag{4.1}$$

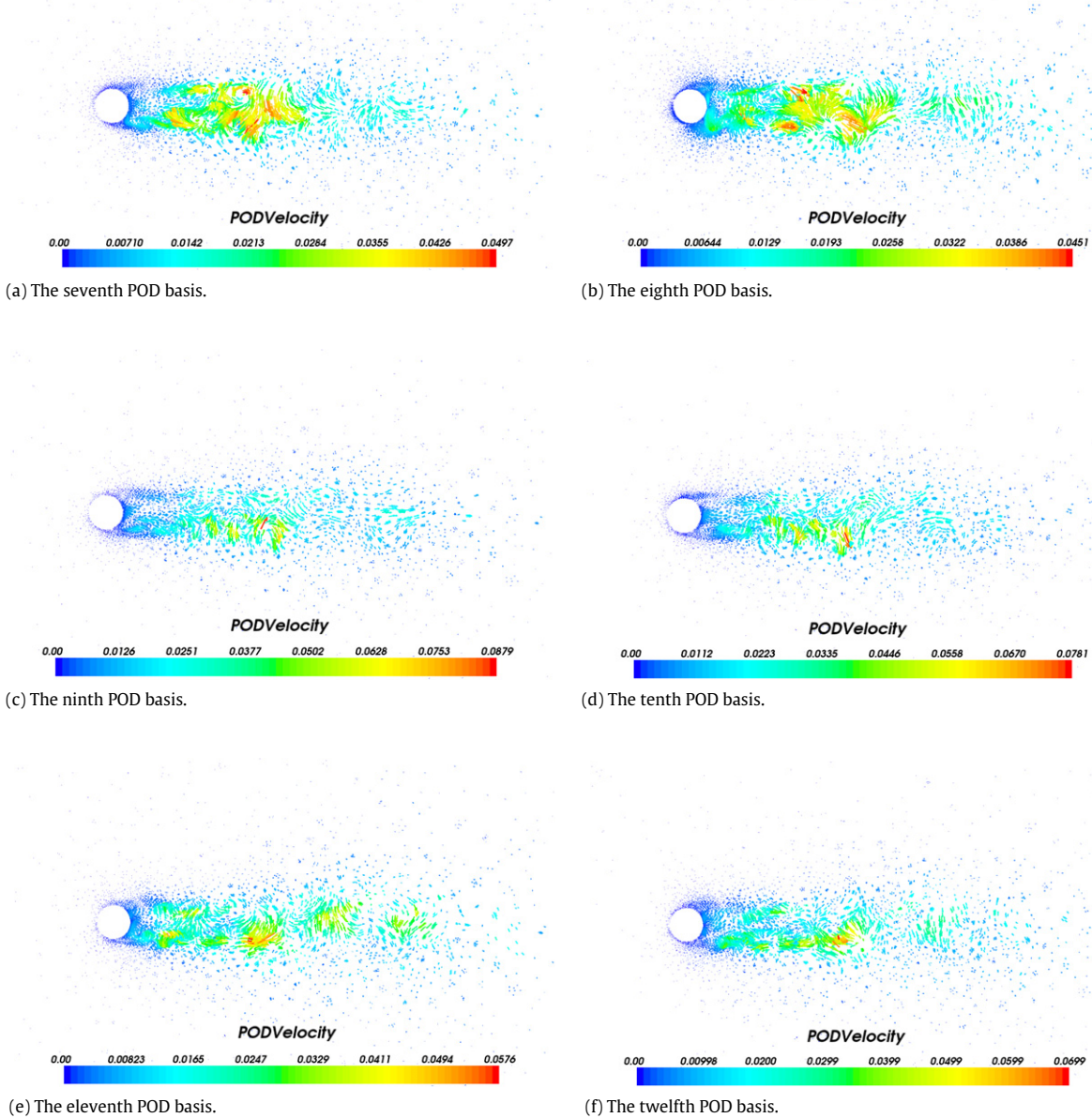
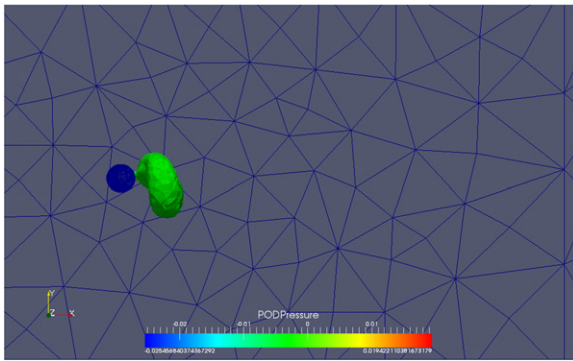


Fig. 12. The 7th to 12th POD basis functions of velocity.

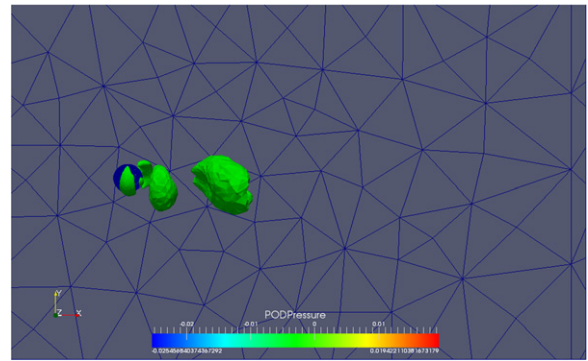
where $\beta = 1.8 \times 10^{-11}$ and the reference density $\rho_0 = 1000 \text{ kg m}^{-3}$. Thus the velocity scale $U = 3.5 \times 10^{-2} \text{ m s}^{-1}$ is used here. Time is non-dimensionalized with $T = L/U$. The non-dimensional wind stress (applied as a body force here averaged over the depth of the domain) takes the same cosine of latitude profile with $\tau_0^* = \tau_0 L / (U^2 \rho_0 H) = 163.2653$. The Coriolis terms are taken into account with the beta-plane approximation ($f = \beta y$). Incorporating the beta-plane approximation yields a non-dimensional $\beta^* = L^2 \beta / U = 514.286$. The spin-up period is 0.3024. The simulation period is [0.3024, 0.6048]. The unstructured mesh adopted consists of 2667 nodes and 5448 elements (Fig. 1). The smallest element side length is 0.02.

Fig. 2 presents the first and second POD basis functions of the two components of the velocity, and we can see that the first POD basis function captures the dominant characteristics of the solution. Fig. 3 illustrates the first and second POD basis functions of the velocity vector. Fig. 4 presents the first and second POD basis functions of the pressure.

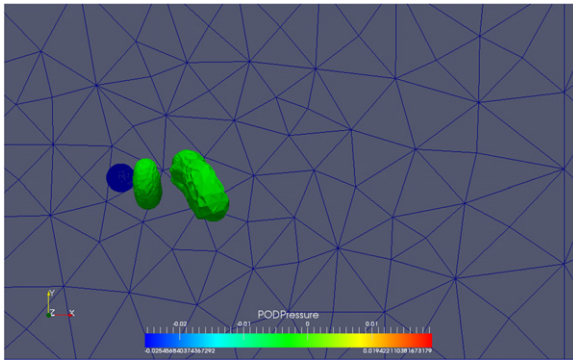
The full model solution and the POD reduced order solution of the velocity and pressure at $t = 0.16$ are presented in Fig. 5, which demonstrate the feasibility and accuracy of the POD reduced order model.



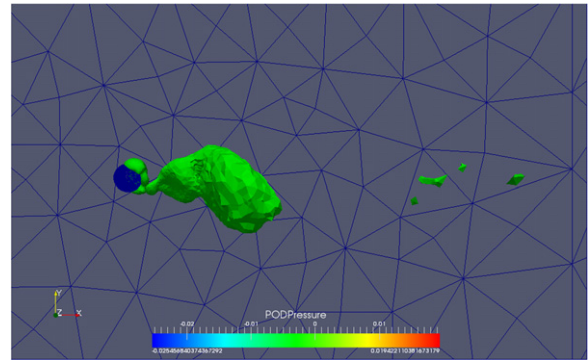
(a) The first POD basis.



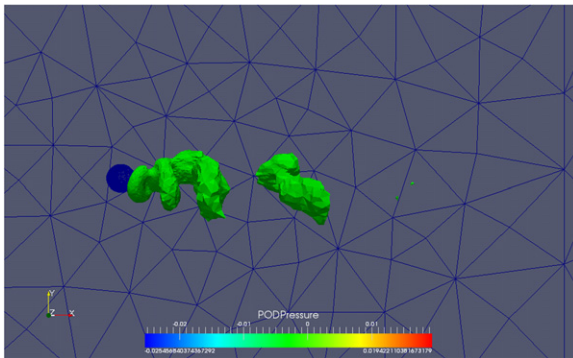
(b) The second POD basis.



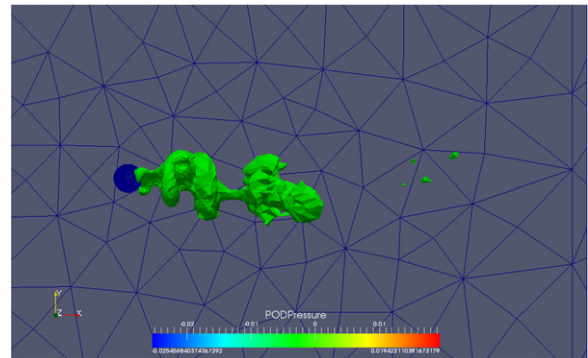
(c) The third POD basis.



(d) The fourth POD basis.



(e) The fifth POD basis.



(f) The sixth POD basis.

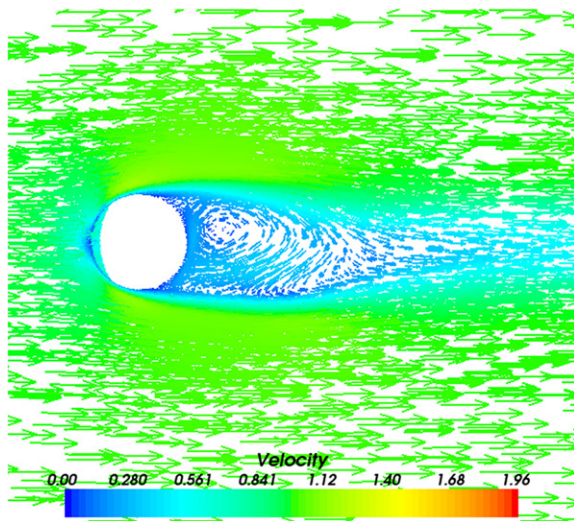
Fig. 13. The first 6 POD basis functions of pressure.

The SVD eigenvalues of the velocity and pressure for the POD reduced order model are presented in Fig. 6 in a decreasing order. We apply the first six POD basis functions of the velocity and pressure to construct the POD reduced order model, which captures more than 99.9% of the total energy.

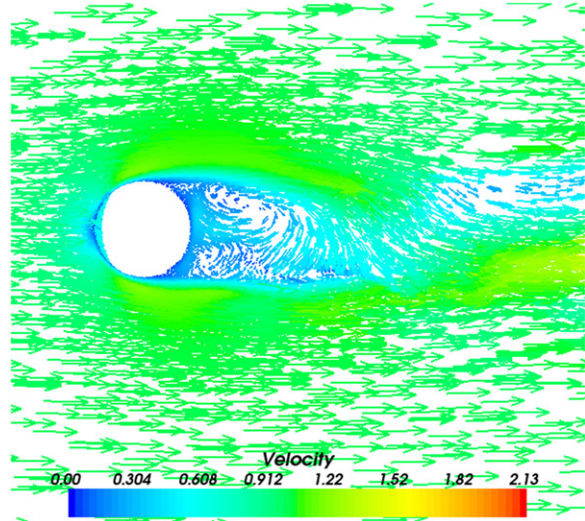
In the present approach, we have the discretized finite element model first and then apply the model reduction method of POD only by some matrix manipulations. The traditional application of the POD method (reduce, then discretize) to the same finite element unstructured mesh ocean model can be found in [13].

4.2. The lock exchange case

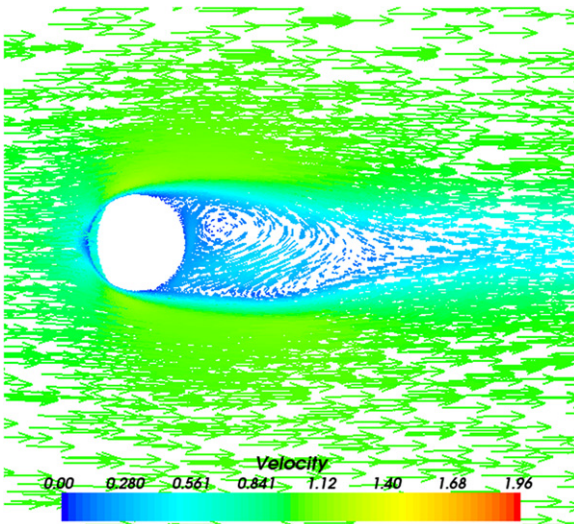
In the lock-exchange two fluids of different density, namely hot and cold fluids, are initially separated by a gate (or 'lock'). The gate is removed and two gravity currents propagate horizontally along the tank. This laboratory-scale set up incorporates dynamics observed in gravity currents over a range of scales [28].



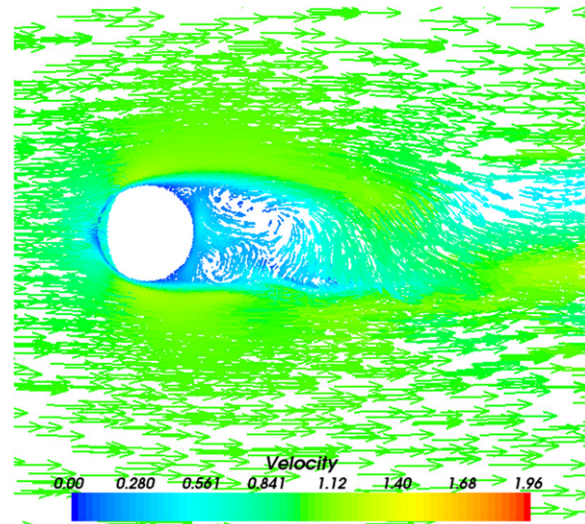
(a) The full-order solution of velocity at $t = 7.5$.



(b) The reduced-order solution of velocity at $t = 7.5$.



(c) The full-order solution of velocity at $t = 10$.



(d) The reduced-order solution of velocity at $t = 10$.

Fig. 14. The full model solution and the reduced order solution of velocity at $t = 7.5$, $t = 10$ and $t = 20$.

The computation region is a non-dimensional rectangle of the size 0.8×0.1 . The unstructured mesh adopted consists of 4040 nodes and 7638 elements. The smallest element side length is 0.005. The initial condition for the velocity and pressure is $u = 0$ and $p = 0$. The initial condition for the non-dimensional temperature is $T = -0.5$ for the cold fluid at the left side of the lock and $T = 0.5$ for the hot fluid at the right side of the lock. The isotropic value of viscosity is 1×10^{-6} . The Crank–Nicolson method is applied in the temporal discretization. The time step is 0.025. The continuous Galerkin projection is applied in the finite element scheme for the state variables. In this case, temperature is computed using a high resolution control volume finite element scheme in the full order model, and the thermal expansion coefficient is 10^{-3} . Fig. 7 shows the full order solution of temperature at $t = 10$ and $t = 16$. For the present research, the POD model reduction method is only applied to the velocity and pressure variables. The POD reduced order model related to the temperature will be developed in future work.

The first and second POD basis functions of velocity and pressure are presented in Fig. 8 respectively. The first six POD basis functions are applied in the reduced order model which can capture more than 99% of the total energy. Fig. 9 shows the full order solution and reduced order solution of velocity for the lock exchange case at $t = 10$ and $t = 16$ respectively.

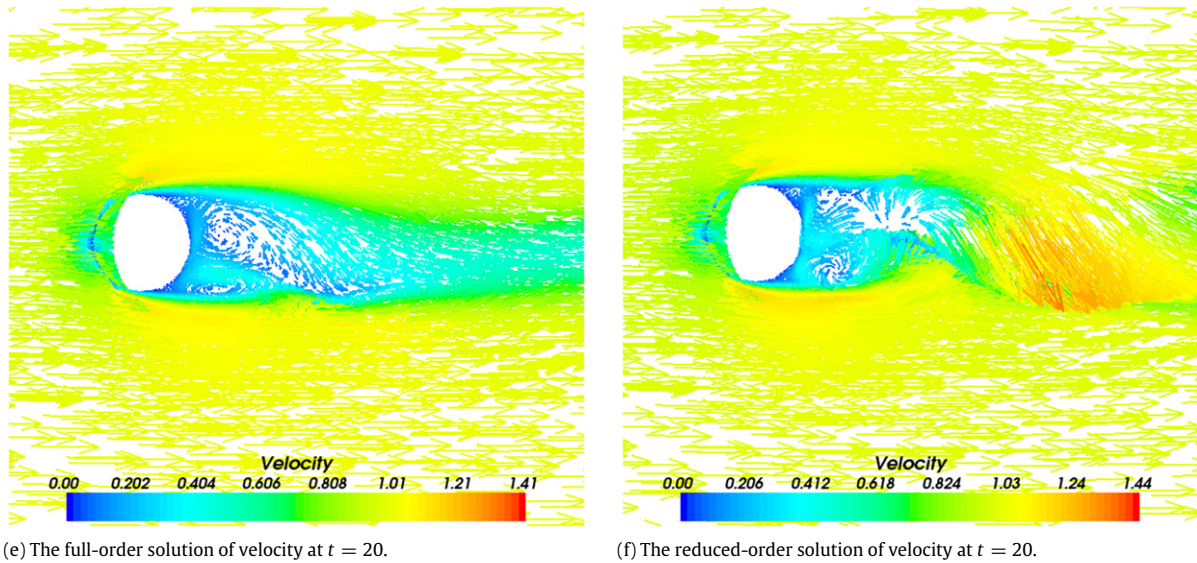


Fig. 14. (continued)

4.3. Three dimensional case of flow past a sphere with moderate Reynolds numbers

For the 3D model of flow past a sphere with the Reynolds number $Re = 400$ is adopted here. The sphere is of unit diameter centered at the origin. The entire domain is the cuboid defined by $-10 \leq x \leq 20$, $-10 \leq y \leq 10$, $-10 \leq z \leq 10$.

The unsteady momentum equations with nonlinear advection and viscous terms along with the incompressibility constraint are numerically solved. Free slip velocity boundary conditions are applied at the four lateral boundaries, $u = 1$, $v = w = 0$ is applied at the inflow boundary $x = -10$, and a free stress boundary condition is applied to the outflow at $x = 20$. The simulation period for the POD reduced order model is during time interval $[44.43, 60]$. The time step is chosen as 0.098.

Adaptive mesh refinement is an efficient way to reduce computational complexity and to provide high resolution snapshots for the reduced order model. For complex simulations starting with a uniform mesh, adaptive mesh refinement can be first adopted to achieve a relatively fine mesh. After that, we can fix the mesh and apply the POD method to reduced the model dimension. An adaptive mesh simulation with an initial mesh of 24 973 points and 141 498 elements as well as an adaptive time step with an initial time step of 0.001 is carried out for the spin-up process of this case.

The three dimensional unstructured mesh in the case of flow past the sphere is shown in Fig. 10(a) and the cut plane at the center of the cuboid is shown in Fig. 10(b). The three dimensional unstructured mesh adopted consists of 47 593 nodes and 261 791 elements.

For the POD reduced order model, the first 12 POD basis functions of velocity at the cut plane in the center of the cuboid are presented in Figs. 11 and 12 in a descending order of magnitude of the corresponding eigenvalues. We can see that the POD basis functions corresponding to smaller eigenvalues contain more eddies. A three dimensional illustration showing the first 6 POD basis functions for the pressure variable is presented in Fig. 13.

The full order solution and POD reduced order solution of the velocity vector around the sphere at different time levels ($t = 7.5$, $t = 10$ and $t = 20$) are showed in Fig. 14 to illustrate the feasibility of the POD reduced order model.

In Fig. 15, the full order solution and POD reduced order solution of velocity and pressure at $t = 35$ are presented. Errors between the full order solution and the reduced order solutions are also presented in Fig. 16, respectively.

4.4. CPU time analysis

The model reduction approach proposed in this work is to derive the POD reduced order model by projecting the matrix and source term vector of the full discrete model onto the reduced space. The implementation of reduced order modeling codes involves only the matrix vector multiplication of the full model. Importantly, the code is largely independent of the implementation details of the original equations. For nonlinear problems, a perturbation approach is used to help accelerate the matrix equation assembly process, based on the assumption that the discretized system of equations has a polynomial representation and can thus be created by a summation of pre-formed matrices.

As shown in Table 1, for Case 1 (the 2D gyre case), the CPU time cost every timestep for the full order model is about 0.8 s. For the new approach, there is no need to rewrite any codes related to the original equations. The reduced order model setup process (preparation of the perturbed POD reduced matrices) at the beginning of the computation cost 5.24 s and the

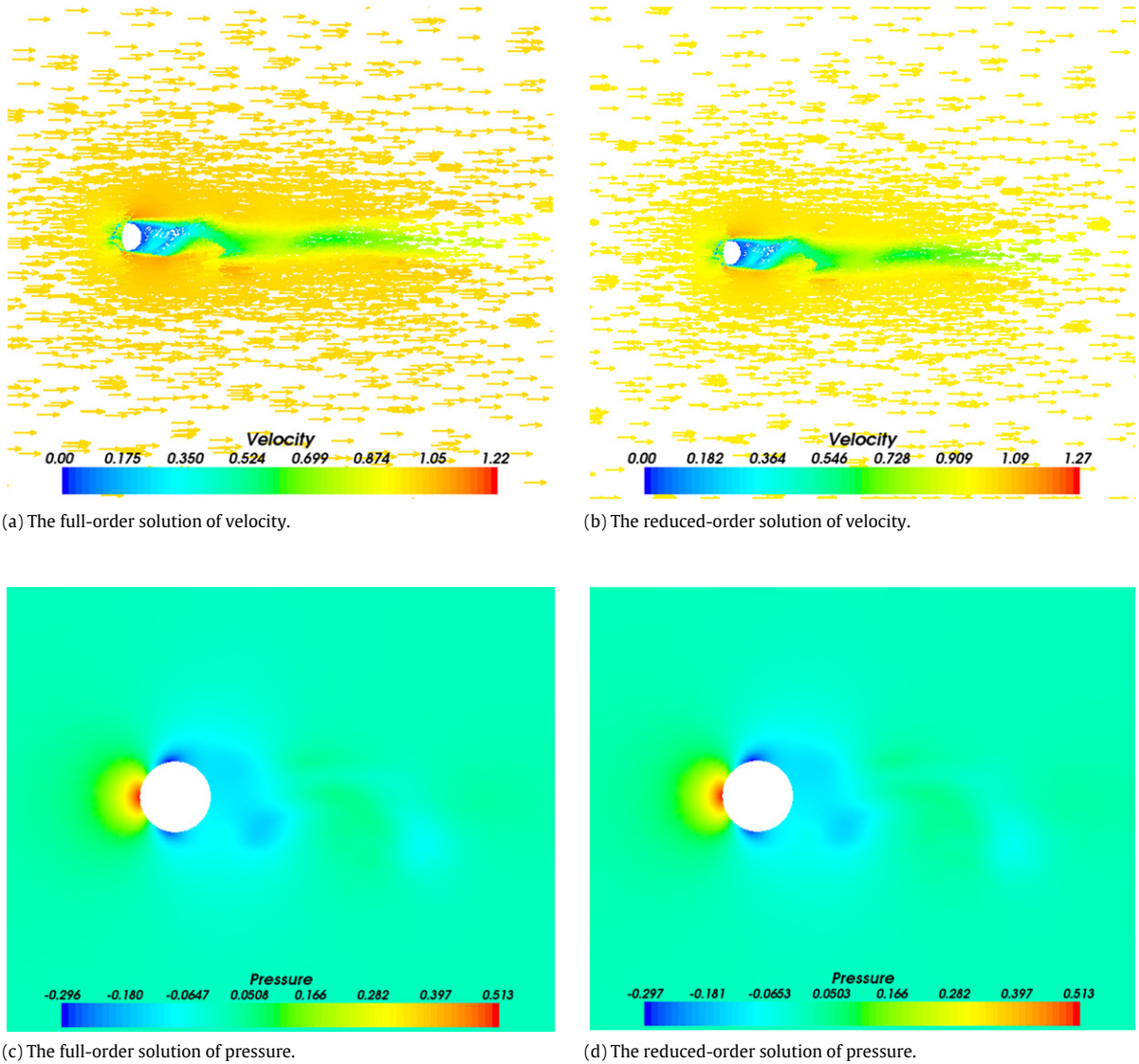


Fig. 15. The full model solution and the reduced order solution of velocity and pressure at $t = 35$.

solution process for every timestep is only 10^{-2} which is about 1/80 of the full order model. Considering the present test case with 30 timesteps carried out, the solution process of the full model costs 24.42 s while the POD reduced order model costs 5.84 s totally. It's because the full order matrix assembling process will not be carried out once the reduced order model setup process is completed.

For Case 2 (the 2D lock exchange case) in Table 1, the POD reduced order model of the lock exchange case costs 17.62 s, which is about 1/25 of the CPU time required by the full order model, namely 403.04 s. If the time spent on the reduced order model setup process is excluded, the CPU time consumed by the reduced order model is only about 1/30 of that consumed by the full order model.

For Case 3 (the 3D flow past sphere case) in Table 1, the CPU time consumed by the POD reduced order model is about 1/40 of that consumed by the full order finite element model, which is of the same order as the model reduction results in [17]. The CPU time of solving the POD reduced order model for every timestep is about 1/500 of that required by the full order model.

From the three test cases, we can see that the efficiency of the POD method applied to the new approach grows with the complexity of the simulation (the number of nodes) and the simulation time. The CPU time consumed by the reduced order model can be reduced to about 10^{-2} of the full order model with the new approach applied to the quadratic nonlinear case. Further research will investigate impact of DEIM methodology on obtaining additional economy in the CPU time for high order nonlinear cases.

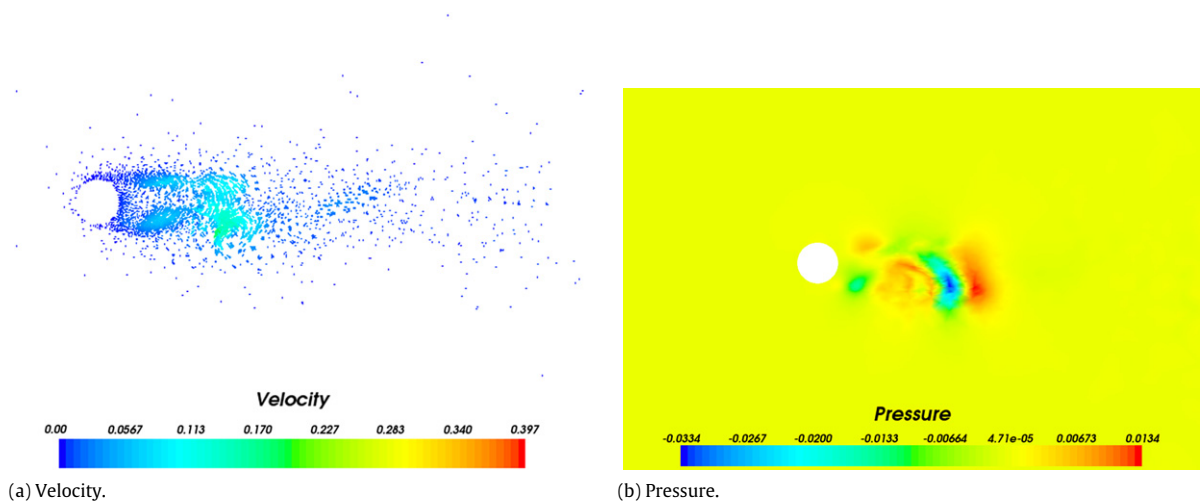


Fig. 16. Error between the full model solution and the reduced order solution.

Table 1
CPU time(s) analysis.

		ROM setup	Solving	Projecting back	Total
Case 1	Full model	0	24.42	0	24.42
	POD ROM	5.24	0.32	0.28	5.84
Case 2	Full model	0	403.04	0	403.04
	POD ROM	3.02	8.32	6.28	17.62
Case 3	Full model	0	15 480	0	15 480
	POD ROM	352.02	30.23	18.61	400.86

5. Summary and conclusions

In this paper, the POD reduced order model is implemented for a finite element fluid model using an unstructured mesh, and is successfully applied to three dimensional flows using the unstructured mesh finite element model. A new scheme for the POD based reduced order model of complex mesh-based numerical models (e.g. finite element unstructured mesh models) is presented. The matrix and source term vector of the full model are projected onto the reduced bases. The POD method is used to form the reduced bases. Implementation of reduced order modeling codes involves only the matrix vector multiplication of the full model. The reduced order modeling code is simple to implement even for complex governing equations, discretization methods and nonlinear parameterizations. Importantly, the code is independent of the implementation details of the full model code. For nonlinear problems, a perturbation approach is used to help accelerate the matrix equation assembly process based on the assumption that the discretized system of equations has a polynomial representation and can thus be formed by a summation of pre-formed matrices. The feasibility and accuracy of the reduced order model applied to three dimensional fluid flows is demonstrated.

Further research will investigate the impact of DEIM methodology on obtaining additional economy in CPU time (due to nonlinear effects); investigate the necessity for a nonlinear turbulence closure POD methodology [29–32]; compare the impact of retention of more basis functions; address the issue of adaptive mesh refinement and POD model reduction; consider the inverse POD 4-D VAR method with and without DEIM; address uncertainty quantification combined with model reduction in framework of fluidity; and finally combine EnKF with POD for using Fluidity-ICOM ocean model and compare with the SEIK filter.

Acknowledgments

This work was carried out under funding from the UK's Natural Environment Research Council (projects NER/A/S/2003/00595, NE/C52101X/1 and NE/C51829X/1), the Engineering and Physical Sciences Research Council (GR/R60898 and EP/I00405X/1), the Imperial College High Performance Computing Service and the Grantham Institute for Climate Change. Juan Du acknowledges the financial support of the Institute of Atmospheric Physics Chinese Academy of Sciences. Prof. I.M. Navon acknowledges the support of NSF/CMG grant ATM-0931198. Prof. J. Zhu acknowledges the support of National Natural Science Foundation (Grant No. 41075064) and National Basic Research Program of China (Grant No. 2012CB417404). Many thanks to Dr G. Gorman for his support. The authors acknowledge the constructive remarks of two anonymous reviewers that contributed to the improvement and clarification of the present manuscript.

References

- [1] A.C. Antoulas, Approximation of Large Scale Dynamical System, Society for Industrial and Applied Mathematics, 2005.
- [2] M.J. Rewienski, A trajectory piecewise-linear approach to model order reduction of nonlinear dynamical systems, Ph.D. Thesis, Massachusetts Institute of Technology, Cambridge, Massachusetts.
- [3] K. Fukunaga, Introduction to Statistical Recognition, second ed., in: Computer Science and Scientific Computing Series, Academic Press, Boston, MA, 1990.
- [4] I.T. Jolliffe, Principal Component Analysis, Springer, Berlin, 2002.
- [5] D.T. Crommelin, A.J. Majda, Strategies for model reduction: comparing different optimal bases, *Journal of the Atmospheric Sciences* 61 (2004) 2206–2217.
- [6] A.J. Majda, I. Timofeyev, E. Vanden-Eijnden, Systematic strategies for stochastic mode reduction in climate, *Journal of the Atmospheric Sciences* 60 (2003) 1705–1723.
- [7] J. Du, J. Zhu, Z.D. Luo, I.M. Navon, An optimizing finite difference scheme based on proper orthogonal decomposition for CVD equations, *Communications in Numerical Methods in Engineering* 27 (1) (2011) 78–94.
- [8] Z. Luo, J. Chen, J. Zhu, R. Wang, I.M. Navon, An optimizing reduced order FDS for the tropical Pacific Ocean reduced gravity model, *International Journal for Numerical Methods in Fluids* 55 (2) (2007) 143–161.
- [9] Z. Luo, R. Wang, J. Zhu, Finite difference scheme based on proper orthogonal decomposition for the non-stationary Navier–Stokes equations, *Science in China Series A: Mathematics* 50 (8) (2007) 1186–1196.
- [10] Z. Luo, J. Zhu, R. Wang, I.M. Navon, Proper orthogonal decomposition approach and error estimation of mixed finite element methods for the tropical Pacific Ocean reduced gravity model, *Computer Methods in Applied Mechanics and Engineering* 196 (41–44) (2007) 4184–4195.
- [11] Y. Cao, J. Zhu, Z. Luo, I.M. Navon, Reduced order modeling of the upper tropical Pacific Ocean model using proper orthogonal decomposition, *Computers and Mathematics with Applications* 52 (2006) 1373–1386.
- [12] Y. Cao, J. Zhu, I.M. Navon, Z. Luo, A reduced order approach to four-dimensional variational data assimilation using proper orthogonal decomposition, *International Journal for Numerical Methods in Fluids* 53 (2007) 1571–1583.
- [13] F. Fang, C.C. Pain, I.M. Navon, M.D. Piggott, G.J. Gorman, P.A. Allison, A.J.H. Goddard, Reduced-order modelling of an adaptive mesh ocean model, *International Journal for Numerical Methods in Fluids* 59 (2009) 827–851.
- [14] M. Barrault, Y. Maday, N.C. Nguyen, A.T. Patera, An ‘empirical interpolation’ method: application to efficient reduced-basis discretization of partial differential equations, *Comptes Rendus Mathematique* 339 (9) (2004) 667–672.
- [15] S. Chaturantabut, D.C. Sorensen, Nonlinear model reduction via discrete empirical interpolation, *SIAM Journal on Scientific Computing* 32 (5) (2010) 2737–2764.
- [16] Z. Wang, I. Akhtar, J. Borggaard, T. Iliescu, Proper orthogonal decomposition closure models for turbulent flows: a numerical comparison, *Computer Methods in Applied Mechanics and Engineering* 237–240 (2012) 10–26.
- [17] S. Chaturantabut, D.C. Sorensen, Application of POD and DEIM on dimension reduction of non-linear miscible viscous fingering in porous media, *Mathematical and Computer Modelling of Dynamical Systems* 17 (4) (2011) 337–353.
- [18] A.R. Kellems, S. Chaturantabut, D.C. Sorensen, S.J. Cox, Morphologically accurate reduced order modelling of spiking neurons, *Journal of Computational Neuroscience* 28 (3) (2010) 477–494.
- [19] C.C. Pain, M.D. Piggott, A.J.H. Goddard, F. Fang, G.J. Gorman, D.P. Marshall, M.D. Eaton, P.W. Power, C.R.E. de Oliveira, Three-dimensional unstructured mesh ocean modelling, *Ocean Modelling* 10 (1–2) (2005) 5–33.
- [20] R. Ford, C.C. Pain, M.D. Piggott, A.J.H. Goddard, C.R.E. de Oliveira, A.P. Umbleby, A nonhydrostatic finite-element model for three-dimensional stratified oceanic flows. Part I: model formulation, *Monthly Weather Review* 132 (12) (2004) 2816–2831.
- [21] J. Blum, F.X. Le Dimet, I.M. Navon, Data Assimilation for Geophysical Fluids. Chapter in *Computational Methods for the Atmosphere and the Oceans*, in: R. Temam, J. Tribbia (Guest Editors), Special Volume of Handbook of Numerical Analysis, vol. 14, Elsevier Science Ltd., New York, 2009, p. 784. ISBN-13: 978-0444518934 (Philippe G. Ciarlet (Ed.)).
- [22] P. Moin, R.D. Moser, Characteristic-eddy decomposition of turbulence in channel, *Journal of Fluid Mechanics* 200 (1989) 417–509.
- [23] R.D. Joslin, M.D. Gunzburger, R.A. Nicolaidis, G. Erlebacher, M.Y. Hussaini, A self-contained automated methodology for optimal flow control validated for transition delay, *AIAA Journal* 35 (1997) 816–824.
- [24] H.V. Ly, H.T. Tran, Proper orthogonal decomposition for flow calculations and optimal control in a horizontal CVD reactor, *Quarterly of Applied Mathematics* 60 (2002) 631–656.
- [25] D. Ahlman, F. Södelund, J. Jackson, A. Kurdila, W. Shyy, Proper orthogonal decomposition for time-dependent lid-driven cavity flows, *Numerical Heat Transfer, Part B—Fundamentals* 42 (2002) 285–306.
- [26] J. Du, I.M. Navon, J.L. Steward, A.K. Alekseev, Reduced-order modeling based on POD of a parabolized Navier–Stokes equation model I: forward model, *International Journal for Numerical Methods in Fluids* 69 (3) (2012) 710–730.
- [27] F. Fang, C.C. Pain, I.M. Navon, M.D. Piggott, G.J. Gorman, P.E. Farrell, P.A. Allison, A.J.H. Goddard, A POD reduced-order 4D-Var adaptive mesh ocean modelling approach, *International Journal for Numerical Methods in Fluids* 60 (2009) 709–732.
- [28] T.B. Benjamin, Gravity currents and related phenomena, *Journal of Fluid Mechanics* 31 (1968) 209–248.
- [29] O. San, A.E. Staples, Z. Wang, T. Iliescu, Approximate deconvolution large eddy simulation of a barotropic ocean circulation model, *Ocean Modelling* 40 (2011) 120–132.
- [30] I. Akhtar, Z. Wang, J. Borggaard, T. Iliescu, Jacobian based nonlinear closure for reduced-order models, *Journal of Computational Nonlinear Dynamics* 7 (3) (2012) 034503.
- [31] T. Iliescu, Z. Wang, Variational multiscale proper orthogonal decomposition: convection-dominated convection–diffusion equations, *Mathematics of Computation* (2012) (in press). Available on arXiv:1103.2729.
- [32] J. Huang, Z. Wang, R. Zhu, Asymptotic error expansions for hypersingular integrals, *Advances in Computational Mathematics* (2011), on line first (<http://dx.doi.org/10.1007/s10444-011-9236-x>).